



Chapter 2

Human osteochondral explants: reliable biomimetic models to investigate disease mechanisms and develop personalized treatments for Osteoarthritis

Evelyn Houtman¹, Marcella van Hoolwerff¹, Nico Lakenberg¹, Eka H.D. Suchiman¹, Enrike van der Linden-van der Zwaag², Rob G.H.H Nelissen², Yolande F.M Ramos¹, Ingrid Meulenbelt¹

¹*Molecular Epidemiology, Department of Biomedical Data Sciences, Leiden University Medical Center, Leiden, The Netherlands.*

²*Department of Orthopaedics, Leiden University Medical Center, Leiden, The Netherlands.*

Published in: *Rheumatology and Therapy*. 2021 Mar;8(1):499-515.
doi: 10.1007/s40744-021-00287-y

Abstract

Introduction

Likely due to ignored heterogeneity in disease pathophysiology, osteoarthritis (OA) has become the most common disabling joint disease without effective disease modifying treatment causing a large social and economic burden. In this study we set out to explore responses of aged human osteochondral explants upon different OA-related perturbing triggers (inflammation, hypertrophy and mechanical stress) for future tailored biomimetic human models.

Methods

Human osteochondral explants were treated with IL-1 β (10 ng/ml) or triiodothyronine (T3; 10 nM) or received 65% strains of mechanical stress (65% MS). Changes in chondrocyte signalling were determined by expression levels of nine genes involved in catabolism, anabolism and hypertrophy. Breakdown of cartilage was measured by sulphated glycosaminoglycans (sGAGs) release, scoring histological changes (Mankin score) and mechanical properties of cartilage.

Results

All three perturbations (IL-1 β , T3 and 65% MS) resulted in upregulation of the catabolic genes *MMP13* and *EPAS1*. IL-1 β abolished *COL2A1* and *ACAN* gene expression and increased cartilage degeneration, reflected by increased Mankin scores and sGAGs released. Treatment with T3 resulted in a high and significant upregulation of the hypertrophic markers *COL1A1*, *COL10A1*, and *ALPL*. However, 65% MS increased sGAG release and detrimentally altered mechanical properties of cartilage.

Conclusion

We present consistent and specific output on three different triggers of OA. Perturbation with the pro-inflammatory IL-1 β mainly induced catabolic chondrocyte signalling and cartilage breakdown, while T3 initiated expression of hypertrophic and mineralization markers. Mechanical stress at a strain of 65% induced catabolic chondrocyte signalling and changed cartilage matrix integrity. The major strength of our *ex vivo* models was that they considered aged, preserved, human cartilage of a heterogeneous OA patient population. As a result, the explants may reflect a reliable biomimetic model prone to OA onset allowing for development of different treatment modalities.

Keywords

cartilage, osteochondral explants, osteoarthritis, human biomimetic model, mechanical stress, hypertrophy, inflammation.

Introduction

Osteoarthritis (OA) is the most prevalent chronic age-related joint disease, causing pain and disability [1]. Likely due to ignored heterogeneity in disease pathophysiology, osteoarthritis has become the most common disabling joint disease without effective disease-modifying OA drugs (DMOADs) causing great social and economic burdens. As a result, OA significantly decreases quality of life while increasing absenteeism from work, and healthcare costs [2].

The OA disease process itself is characterized by unfavourable dynamic regulation of chondrocytes upon environmental perturbations such as age or mechanical stress, likely in interaction with genetic variants that cause subtle changes in expression of OA risk genes. The OA pathophysiological process itself has been linked to enhanced metabolic activity of articular chondrocytes, resembling growth plate chondrocytes undergoing endochondral ossification [3]. OA chondrocytes enter a cascade of proliferation and hypertrophic differentiation, accompanied by expression of genes such as alkaline phosphatase (*ALPL*), collagen X (*COL10A1*) and matrix metalloproteinase 13 (*MMP13*), resulting in apoptotic death and mineralization of cartilage [4-8]. Other hallmarks of the OA disease pathophysiology include new bone formation at the joint margins, limited inflammation and changes in subchondral bone structure. Together, these OA risk factors impose a persistent, yet variable, negative influence on joint tissue homeostasis throughout life, inevitably leading to progressive joint tissue destruction with age [9].

To address shortcomings of translational research and the challenges of translating data from *in vitro* models and a preclinical animal model to humans and increase efficiency of effective and safe drug development, while being compliant with the guiding principles of reduction, refinement and replacement of animal experiments, validated human models mimicking the different aspects of OA pathophysiology are required. Nonetheless, preclinical models thus far are limited to post-traumatic animal models or analyses of cell signalling in 2D and 3D *in vitro* cultures of neo-cartilage derived from human articular chondrocytes or stem cells. However, none of these models reliably recapitulate the osteochondral compartment, let alone faithfully representing age-related joint tissues prone to enter the OA process upon disease-initiating cues.

Osteochondral explant-based models allow investigation of both bone and cartilage compartments at the same time. The major advantage of such a model is that the cell response can be determined in their natural environment and they are relatively simple and easy to produce. Most commonly used explant-based models thus far were of bovine origin and applied a super-physiological perturbing factor of either a fierce inflammatory cytokines treatment [10-12] or cartilage loading [13-15]. Next to inflammation and mechanical loading, recapitulation of endochondral ossification and thereby hypertrophy is also thought to be one of the major mechanisms driving the processes in OA [16].

The aim of the current study is to explore and compare responses of aged human osteochondral explants triggered by three different physiological perturbing cues: inflammation (IL-1 β) [17,18], hypertrophy (triiodothyronine (T3)) [19,20] and mechanical stress (65% strain) [21].

We determined different output measures related to catabolic, anabolic and hypertrophic chondrocyte signalling, sGAGs released into the media, cartilage structure by histology and changes in mechanical properties. The presented models enable in-depth studies on how such cues interfering with homeostasis of aged cartilage contribute to human OA onset. They also allow for personalized testing of new treatment regimes in a validated human model including interaction of joint tissues and essential environmental cues.

Material and Methods

Osteochondral explant cultures

Osteochondral explants were obtained from joints included in the Research in Articular Osteoarthritis Cartilage (RAAK) study. The RAAK study was approved by the medical ethics committee of the Leiden University Medical Center (Po8.239/P19.013) and informed consent was obtained from subjects. Osteochondral explants were harvested from the macroscopically preserved area of knee joints of human OA patients, within 2 hours of joint replacement surgery. Donor characteristics are summarized in **Table S1**. Osteochondral explants containing both cartilage and bone (8 mm diameter) were washed in sterile PBS and equilibrated in serum-free chondrogenic differentiation medium (DMEM (high glucose; Gibco, Bleiswijk), supplemented with ascorbic acid (50 µg/ml; Sigma-Aldrich; Zwijndrecht, The Netherlands), L-proline (40 µg/ml; Sigma-Aldrich), sodium pyruvate (100 µg/ml; Sigma-Aldrich), dexamethasone (0.1 µM; Sigma-Aldrich), ITS+ and antibiotics (100 U/ml penicillin; 100 µg/ml streptomycin; Gibco)) in a 5% (v/v) CO₂ incubator at 37°C.

Application of physiological relevant cues

Three days after extraction, explant tissue was treated with IL-1β (10 ng/ml) or triiodothyronine (T₃, 10 nM). After 6 days, dynamic unconfined compression was applied to explant tissue using the Mach-1 mechanical testing system on 4 subsequent days (Biomomentum Inc., Laval, QC, Canada). Physiological loading at a strain of 30% or 65% was applied to explants at a frequency of 1 Hz. The thickness of the cartilage was measured prior to loading and used to determine the strain for each explant. Media of explants was refreshed every 3-4 days. To investigate lasting effects of treatment, explants were harvested 3 days after the last treatment. Cartilage and bone were separated using a scalpel, snap-frozen in liquid nitrogen and stored at -80 °C for RNA isolation.

RNA isolation, Reverse Transcription and quantitative Real-Time PCR

RNA was extracted by pulverizing the tissue using a Mixer mill 200 (Retch, Germany) and homogenizing in TRIzol reagent (Invitrogen, San Diego, CA). RNA was extracted with chloroform, precipitated with ethanol and purified using the RNeasy Mini Kit (Qiagen, GmbH, Hilden, Germany). Genomic DNA was removed by DNase (Qiagen, GmbH, Hilden, Germany) digestion and the quantity of RNA was assessed using a Nanodrop spectrophotometer (Thermo Fischer Scientific Inc., Wilmington, DE, USA). Synthesis of cDNA was performed using 200 ng of total mRNA with the First Strand cDNA Synthesis Kit (Roche Applied Science, Almere,

The Netherlands) according to the manufacturer's protocol. Gene expression was determined with the Roche Lightcycler 480 II (Roche Applied Science) using Fast Start Sybr Green Master mix (Roche Applied Science). Primer sequences are listed in **Table S2**.

Sulphated glycosaminoglycan (sGAGs) measurement

Sulphated glycosaminoglycans (sGAGs) concentration was measured with the photometric 1.9 dimethylene blue (DMMB; Sigma-Aldrich) dye method [22]. Shark chondroitin sulphate (Sigma-Aldrich) was used as reference standard. To measure concentrations, absorbance at 525 and 595 was measured in a microplate reader (Synergy HT; BioTek, Winooski, VT, USA).

Histology

Osteochondral explants were fixed in 4% formaldehyde and decalcified using EDTA (12.5%, pH=7.4), dehydrated with an automated tissue processing apparatus and embedded in paraffin. Tissue sections of 5 μm were stained with haematoxylin and eosin (H&E) or toluidine blue (Sigma-Aldrich) and mounted with Pertex (Sigma-Aldrich). Quantification of OA related cartilage damage was scored according to Mankin *et al* [23].

Mechanical properties

The fibril-network-reinforced biphasic model of cartilage in unconfined compression was used to measure the mechanical properties of explants [24]. After a 10% precompression 5 subsequent ramps of 2% were performed and each ramp was allowed to continue until the relaxation rate was < 0.05 N/min. The tensile stiffness of the fibril network (E_v), equilibrium modulus (E_m) and hydraulic permeability (k) were determined using MACH-1 software (Biomomentum Inc., Laval, QC, Canada).

Statistical analysis

Statistics were performed for all data in IBM SPSS statistics 23. In the absence of perfect pairs, the significance of mean difference in gene expression between controls and treated explants was estimated by the generalized estimating equation (GEE) with robust variance estimators to account for donor effects. RT-PCR data were normalized using the housekeeping gene *SDHA*. We used *SDHA*, as this gene was previously identified as a stable housekeeping gene in cartilage and particularly not responsive to mechanical stress [25,26]. Fold changes were calculated according to the $2^{-\Delta\Delta\text{CT}}$ method. Significance was declared at $P < 0.05$.

Results

Baseline characteristics of donors of the osteochondral explants

As shown in **Table S1**, age and BMI are comparable across donors in the three different perturbations applied; IL-1 β , T3 and 65% mechanical stress (65% MS). Of note, IL-1 β was applied by chance in explants from females only. Prior to applying our models we explored effects of 30% stress to osteochondral explants as compared to controls and IL-1 β or T3 treatment. As shown in **Figure S1** and **Figure S2** and **Table S2** and **Table S3**, 30% mechanical stress as compared to controls had no significant effect on gene expression levels, Mankin score or sGAG concentrations (data not published). To enlarge our sample sizes for the remaining analysis, the 30% stressed control samples were pooled with controls of the IL-1 β and T3 treated groups.

Changes in chondrocyte signaling across the three models

As shown in **Table 1**, applying the three different perturbations (IL-1 β , T3 and 65% MS) resulted in significant upregulation of the catabolic genes *MMP13* and *EPAS1* as compared to controls (**Figure 1**). Upregulation of *MMP13* (**Figure 1C**) was modest in response to T3 (FC=3.7; $P=3.0\times 10^{-3}$) relative to that with IL-1 β (FC=12.7; $P=3.6\times 10^{-2}$, **Figure 1A**) and 65% MS (FC=10.3; $P=1.4\times 10^{-2}$, **Figure 1B**). Upregulation of *EPAS1* was highly significant in response to IL-1 β , 65% MS and T3 treatment (FC=4.6; $P=3.6\times 10^{-2}$, FC=1.8; $P=1.8\times 10^{-20}$ and FC=1.8, $P=1.0\times 10^{-3}$, respectively **Figure 1**). Notable is the observed absence in expression changes of the aggrecanase *ADAMTS5* in all three perturbations (**Table 1** and **Figure 1**).

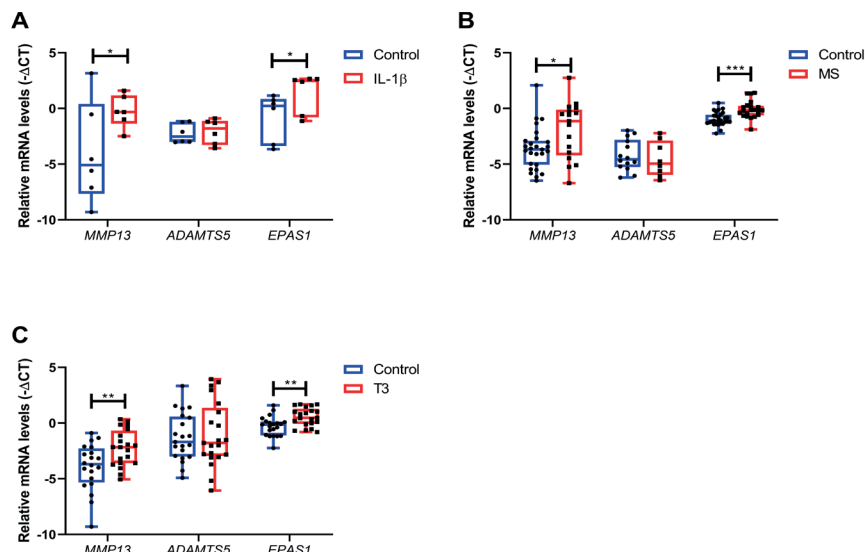


Figure 1 | Gene expression of catabolic markers after treatment with IL-1 β , mechanical stress (MS) or T3. RT-PCR analysis of *MMP13*, *ADAMTS5* and *EPAS1* after [A] IL-1 β (10ng/ml; n=6), [B] 65% MS (n=19-23) or [C] T3 (10nM; n=21) treatment. Data is presented in a boxplot depicting the median, lower and upper quartiles and each dot represents a single explant. P-values of mean differences in gene expression between controls and treated explants were estimated by generalized estimating equations (GEE) with robust variance estimators to account for donor effects. * $P<0.05$, ** $P<0.01$, *** $P<0.001$.

Regarding the matrix genes known to be responsible for a substantial part of the matrix deposition, we showed that *COL2A1* and *ACAN* expression was almost absent in the IL-1 β treated osteochondral explants with a FC=0.01; $P=2.6\times 10^{-12}$ and FC=0.03; $P=1.1\times 10^{-19}$, respectively (**Figure 2A**). 65% MS resulted in a slight, non-significant, downregulation of *COL2A1* (FC=0.9; $P=8.7\times 10^{-2}$, **Figure 2B**) and no changes in *ACAN* expression. In contrast, treatment with T3 resulted in a highly significant upregulation of *COL2A1* (FC=3.5; $P=2.4\times 10^{-10}$, **Figure 2C**). As shown in **Table 1** and **Figure 3C**, treatment with T3 resulted in a high and significant upregulation of the hypertrophic markers *COL1A1* (FC=144.7; $P=0.3\times 10^{-3}$), *COL10A1* (FC=5.0; $P=6\times 10^{-3}$), and *ALPL* (FC=665.8 $P=7.4\times 10^{-9}$) compared to controls.

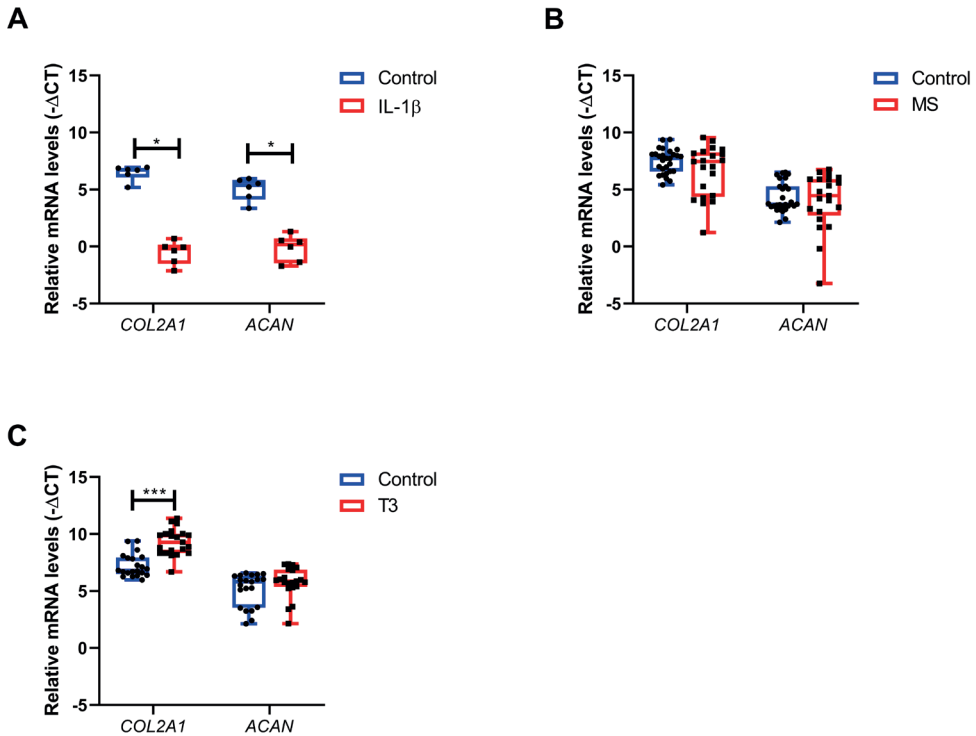


Figure 2 | Gene expression of anabolic markers after treatment with IL-1 β , mechanical stress (MS) or T3. RT-PCR analysis of *COL2A1* and *ACAN* after **[A]** IL-1 β (10ng/ml; n=6), **[B]** 65% MS (n=19-23) or **[C]** T3 (10nM; n=21) treatment. Data is presented in a boxplot depicting the median, lower and upper quartiles and each dot represents a single explant. P-values of mean differences in gene expression between controls and treated explants were estimated by generalized estimating equations (GEE) with robust variance estimators to account for donor effects. * $P<0.05$, ** $P<0.01$, *** $P<0.001$.

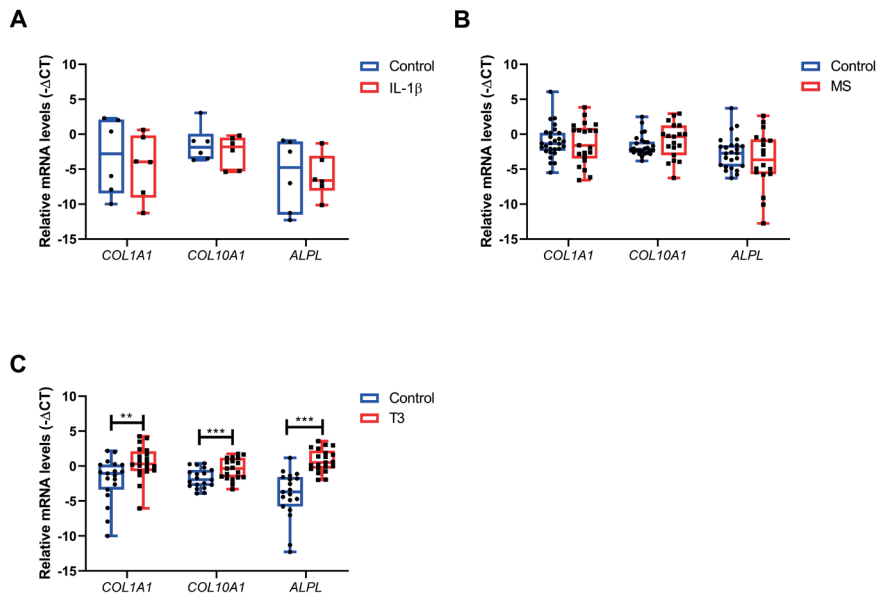


Figure 3 | Gene expression of hypertrophic and mineralization markers after treatment with IL-1 β , mechanical stress (MS) or T₃. RT-PCR analysis of COL1A1, COL10A1 and ALPL after [A] IL-1 β (10ng/ml; n=6), [B] 65% MS (n=19-23) or [C] T₃ (10nM; n=21) treatment. Data is presented in a boxplot depicting the median, lower and upper quartiles and each dot represents a single explant. P-values of mean differences in gene expression between controls and treated explants were estimated by generalized estimating equations (GEE) with robust variance estimators to account for donor effects. *P<0.05, **P<0.01, ***P<0.001.

Table 1 | Summary of the different outcome parameters in response to perturbation with IL-1 β , T₃ or 65% mechanical stress (MS).

Outcome measure	IL-1 β		T ₃		65% MS	
	FC*	P value [§]	FC*	P value [§]	FC*	P value [§]
Gene expression						
Catabolism						
<i>MMP13</i>	12.66	3.60x10 ⁻²	3.74	3.00x10 ⁻³	10.27	1.40x10 ⁻²
<i>ADAMTS5</i>	1.26	NS	0.74	NS	1.04	NS
<i>EPAS1</i>	4.56	3.60x10 ⁻²	1.83	1.00x10 ⁻³	1.77	1.80x10 ⁻²⁰
Anabolism						
<i>ACAN</i>	0.03	1.08x10 ⁻¹⁹	0.97	NS	1.18	NS
<i>COL2A1</i>	0.01	2.56x10 ⁻¹²	3.45	2.40x10 ⁻¹⁰	0.91	NS
Hypertrophy						
<i>COL1A1</i>	0.22	NS	144.68	3.00x10 ⁻³	1.91	NS
<i>COL10A1</i>	0.23	NS	5.04	6.11x10 ⁻³	3.82	NS
<i>ALP</i>	2.80	NS	665.82	7.42 x10 ⁻⁹	2.73	NS
<i>RUNX2</i>	0.68	5.00x10 ⁻²	1.18	NS	1.78	NS

Outcome Measure	IL-1 β		T3		65% MS	
	Beta**	P value ^{\$}	Beta**	P value ^{\$}	Beta**	P value ^{\$}
Histology						
Mankin score						
Cartilage structure	0.83	8.12 x10 ⁻³	0.45	NS	0.20	NS
Cellularity	0.36	NS	0.09	NS	0.04	NS
Toluidine blue	0.79	3.15x10 ⁻³	-0.07	NS	0.16	NS
Tidemark integrity	-0.02	NS	0.06	NS	0.10	NS
Mankin Score	1.95	5.47x10 ⁻⁴	0.53	NS	0.50	NS
sGAG						
Medium						
Day 4	-0.10	NS	23.19	NS	10.21	NS
Day 6	60.51	7.87x10 ⁻²	-1.95	NS	1.56	NS
Day 10	26.48	6.01x10 ⁻³	2.59	NS	7.85	NS
Day 13	59.09	4.85x10 ⁻⁸	1.27	NS	10.31	NS
Cartilage tissue						
Day 13	-1.95	NS	0.04	NS	2.72	NS
Mechanical properties						
Fibril network modulus						
Day 6	-0.11	NS	0.01	NS	-0.07	NS
Day 10	-0.04	NS	0.21	NS	-0.48	2.57x10 ⁻²
Day 13	-0.03	NS	0.19	NS	-0.35	NS
Equilibrium Modulus						
Day 6	-0.02	NS	0.05	NS	-0.02	NS
Day 10	-0.02	NS	0.02	NS	-0.10	2.68x10 ⁻²
Day 13	-0.01	NS	0.08	NS	-0.07	NS
Permeability						
Day 6	6.44	NS	0.93	NS	0.84	NS
Day 10	3.62	NS	4.17	NS	2.46	NS
Day 13	0.71	NS	-2.62	NS	1.45	NS

*FC is determined by the $2^{-\Delta\Delta CT}$ method and compared to its respective controls. **Beta is determined by the GEE during the modelling and represents the difference between the perturbation and control groups. \$ significance of mean difference in gene expression between controls and treated explants were estimated by generalized estimating equation (GEE) with robust variance estimators to account for donor effects. Legend: MS= Mechanical stress; NS= not significant; sGAG=sulphated glycosaminoglycans

sGAG release following cartilage perturbation

To explore breakdown of cartilage, we measured sGAG released by the cartilage in the media on day 3, day 6, day 10 and day 13. In **Figure S3** we outlined the accumulation of sGAG release from explants to the medium between day 3 and 6, and in **Figure 4** between day 6 and 13, representing early and late release, respectively. IL-1 β significantly increased release of sGAG into the medium at day 6 relative to day 3 (19% increase from 194.4 $\mu\text{g/ml}$ to 426.1 $\mu\text{g/ml}$ versus 194.5 $\mu\text{g/ml}$ to 366.0 $\mu\text{g/ml}$; $P=0.03$; **Figure S3A**) compared to controls. This increased release was prolonged at a significant and higher rate at day 10 (52% increase of 51.4 $\mu\text{g/ml}$ versus 77.8 $\mu\text{g/ml}$; $P=6.0 \times 10^{-3}$; **Figure 4A**) and day 13 (99% increase of 59.8 $\mu\text{g/ml}$ versus 118.9 $\mu\text{g/ml}$; $P=4.9 \times 10^{-8}$; **Figure 4A**). Although some increased sGAG release after 65% MS and T3 treatment was observed at day 13, there was no significant difference as compared to controls (30% increase of 32.3 $\mu\text{g/ml}$ versus 42.6 $\mu\text{g/ml}$; $P=0.09$ and 4% increase of 28.8 $\mu\text{g/ml}$ versus 30.0 $\mu\text{g/ml}$; $P=0.8$, respectively; **Figure 4B and 4C**).

Changes of the cartilage integrity observed by histology

To evaluate the microscopic changes in the cartilage tissue quality, we applied Mankin scoring to control and perturbed explants at day 13. As shown in **Figure 5A** and **Table 1**, IL-1 β significantly increased the overall Mankin score (2.7 vs 4.1; $P=6.3 \times 10^{-4}$) compared to controls. Upon investigating the different components of the Mankin score separately (cartilage structure, cellularity, loss of sGAG and integrity of tidemark), it appeared that the difference observed for IL-1 β treatment was mainly driven by differences in cartilage structure such as fibrillations and fissures and loss of sGAGs by toluidine blue staining (1.2 vs 2.0, $P=8.1 \times 10^{-3}$ and 0.4 vs 1.3, $P=3.2 \times 10^{-3}$, respectively **Table 1**, **Figure 5D** and **Figure S4**). Although we observed visible fissures and surface deformations only in explants upon 65% MS (**Figure S5**), suggesting cartilage breakdown, this was not reflected by a significant change in the Mankin scores (**Table 1** and **Figure 5C**).

Changes in mechanical properties of the cartilage

To explore the mechanical properties of cartilage in response to the treatments, we determined three different aspects of mechanical properties available at the MACH1 apparatus on day 6, day 10 and day 13. These aspects were the fibril network modulus (E_f), the equilibrium modulus (E_m) and hydraulic permeability (k), reflecting the tensile stiffness, elastic coefficient (Young's modulus) and water retention respectively. As shown in **Figure 6**, 65% MS significantly negatively affected the fibril network modulus (0.9 vs 0.5 MPa; $P=2.6 \times 10^{-2}$; **Figure 6A**) and equilibrium modulus (0.2 vs 0.1 MPa; $P=2.7 \times 10^{-2}$; **Figure 6B**) at day 10 while simultaneously, though not significantly, increasing the hydraulic permeability of the cartilage by 300% (control vs 65% MS; 0.8 vs 3.2 $\text{mm}^2/\text{MPa}\cdot\text{s}$; $P=0.2$; **Figure 6C**). No significant differences in mechanical properties were detected for IL-1 β and T3 treated osteochondral explants.

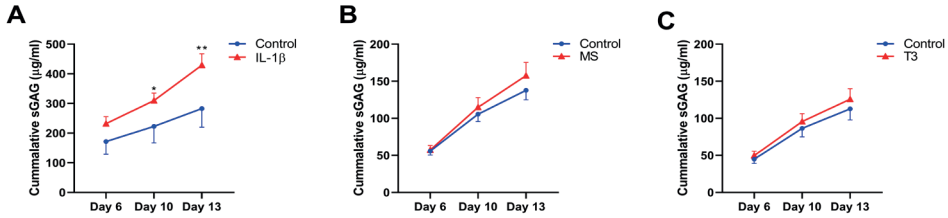


Figure 4 | sGAG concentration in the media of osteochondral explants. Cumulative sGAG release (µg/ml) in media of osteochondral explants in presence of [A] IL-1 β (10ng/ml;n=2), [B] MS (n=19-23) or [C] T3 (10nM; n=17) as determine by the DMMB assay. Data is represented as mean \pm s.e.m. P-values of mean differences between controls and treated explants were estimated by generalized estimating equations (GEE) with robust variance estimators to account for donor effects. *P<0.05, **P<0.01. S.e.m.<0.05 are not distinguishable in the figure.

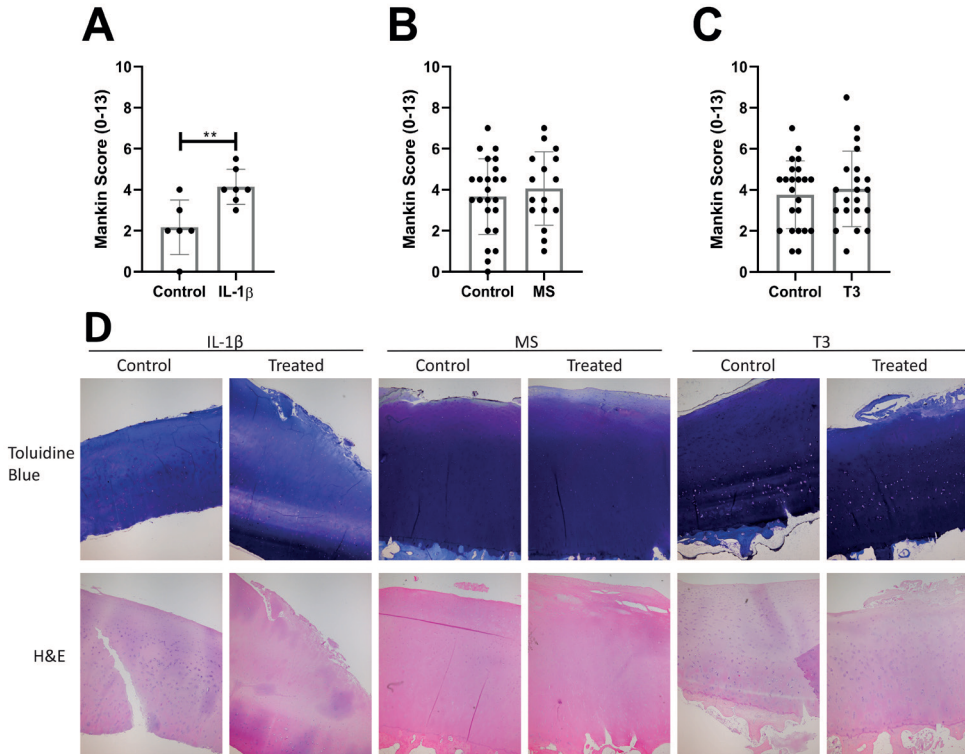


Figure 5 | Mankin Score summary and representative histological pictures of cartilage after treatment with either IL-1 β , T3 or 65% mechanical stress. Cartilage damage was assessed on histology after perturbation with [A] IL-1 β (n=6), [B] 65% MS (n=16/24) or [C] T3 (n=22/24). Data is represented as mean \pm s.e.m and each dot represents a single explant. [D] Representative histological pictures are given of Toluidine blue and H&E stainings performed on slides from the different conditions. P-values of mean differences between controls and treated explants were estimated by generalized estimating equations (GEE) with robust variance estimators to account for donor effects.*P<0.05, **P<0.01.

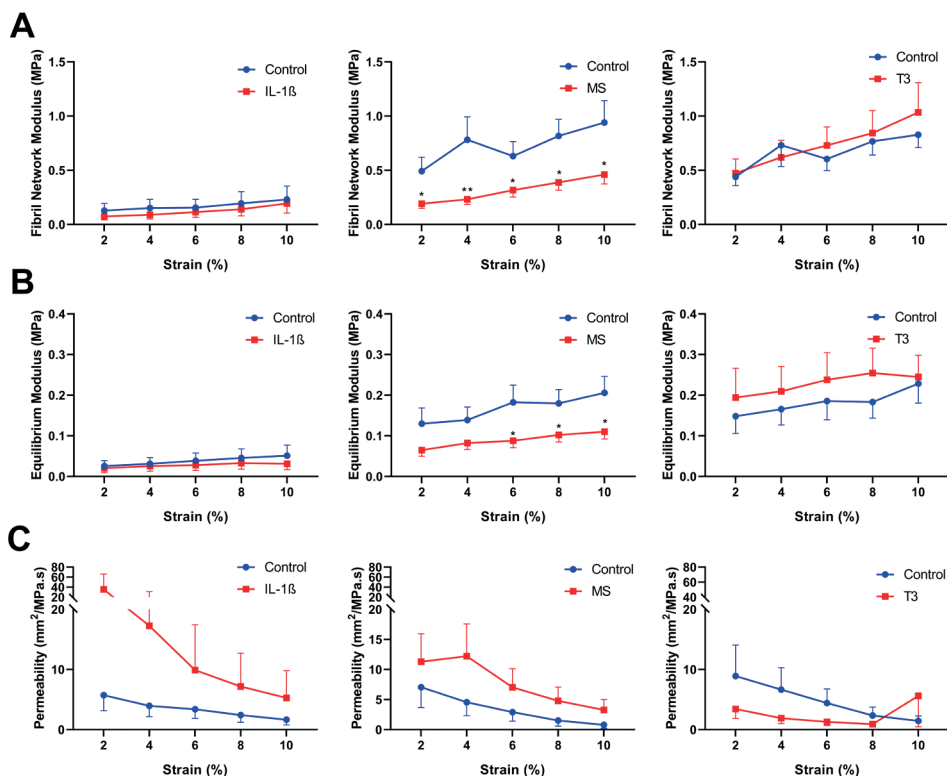


Figure 6 | Mechanical properties of cartilage of osteochondral explants on day 10. Mechanical properties of cartilage was determined after perturbation with IL-1 β (n=3), 65% MS (n=19/21) or T $_3$ (n=19/23) using the fibril-network-reinforced biphasic model to calculate the **[A]** Fibril Network modulus, **[B]** Young's Modulus and **[C]** hydraulic permeability. Data is represented as mean \pm s.e.m. P-values of mean differences between controls and treated explants were estimated by generalized estimating equations (GEE) with robust variance estimators to account for donor effects. *P<0.05, **P<0.01.

Discussion

We present human *ex vivo* osteochondral explants as a model system to study OA related changes after three known pathophysiological perturbations. We applied IL-1 β , T $_3$, and 65% MS as relevant perturbing factors and studied a variety of output measures including chondrocyte signalling, cartilage structure and breakdown, and mechanical properties. Our data provide a relevant personalized human model for research on OA, which can be used for target identification and/or drug efficacy testing. The biomimetic model also complies with the guiding principles of reduction, refinement and replacement of animal experiments.

An increased catabolic response was measured after perturbation in all three models. The highest increase in *MMP13* gene expression was measured in response to IL-1 β (FC=12.7), followed by mechanical stress (FC=10.3), while the lowest increase was observed after T $_3$ treatment (FC=3.7). Strikingly, none of the treatments induced a significant increase in *ADAMTS5* gene expression. Moreover, we measured a greatly significant increase of *EPAS1* in all three OA models, indicating its sensitivity to a perturbed cartilage homeostasis.

The *EPAS1* gene encodes HIF-2 α and its role in the onset of OA in humans is unclear as both increased [27,28] and decreased [29] expression has been reported in human OA cartilage. Functionally, HIF-2 α has been shown to regulate endochondral ossification in mouse studies by inducing expression of genes mediating chondrocyte hypertrophy (*Col10a1*), matrix degradation (*Mmp13*) and vascular invasion (*Vegfa*) [27].

We observed that the three different perturbations were diverse in the other outcome measures. The most severe cartilage breakdown was observed after treatment with the pro-inflammatory IL-1 β and this breakdown was also characterized by an increased chondrocyte cell signalling of catabolism (*MMP13* and *EPAS1*, **Figure 1A**) and abolishment of anabolic cell signalling (*ACAN* and *COL2A1*, **Figure 2A**). Gene expression of *COL2A1* and *ACAN* was downregulated by IL-1 β , 100 and 33 times respectively, suggesting a very low expression of these normally highly expressed cartilage genes. This shift in chondrocyte signalling towards catabolism is confirmed by cartilage breakdown, as measured by a stark 99% increased release of sGAG from cartilage (**Figure 4A**) and by a 1.95 times increased Mankin score (**Figure 5A**). Upon investigation of the different subcategories of the Mankin scoring we observed that IL-1 β greatly reduced cartilage quality as measured by a 3.2 times reduction of staining for sGAG (**Figure S4C**) and 1.7 times increased cartilage surface damage (**Figure S4A**). These results of high cartilage breakdown in response to IL-1 β are in line with many previous studies, which often observed an increased release of matrix metalloproteinases (MMPs) and other degradative enzymes, production of nitric oxide and inhibition of the synthesis of matrix proteins [17,30]. This model might be most suitable to study interventions aimed at a subgroup of OA patients that have more inflammatory characteristics and might even suffer from rheumatic arthritis.

The perturbation with 65% MS can be considered a posttraumatic model, triggering modest OA related changes particularly via catabolism, as reflected by the consistent yet particular effect on *MMP13* and *EPAS1* (FC=1.8; $P=1.8 \times 10^{-20}$ and FC=10.3; $P=1.4 \times 10^{-2}$, respectively). In addition, we showed a slight decrease in cartilage anabolism as measured by reduced *COL2A1* gene expression (FC=0.9; $p=8.7 \times 10^{-3}$). At the protein level we measured a 30% increase of sGAG released from cartilage (**Figure 4C**) after 65% MS, corresponding with the measured slightly higher scoring for sGAG loss in toluidine blue staining (**Figure S4C**). Macroscopically we observed more macrocracks on the cartilage surface (**Figure S5**) of explants receiving 65% MS and this damage was reflected in a substantial unbeneficial change of mechanical properties of the cartilage (**Figure 6**). Compared to controls, explants receiving 65% MS had a 48% reduced tensile stiffness (**Figure 6A**), 55% reduced Young's modulus (**Figure 6B**) and a 300% increased hydraulic permeability (**Figure 6C**). These results suggest that the cartilage extracellular matrix is damaged after 65% MS has been applied as it no longer appears to have the normal elastic properties and water-retaining capabilities that allow cartilage to withstand high loads. We hypothesize that this mechanism of function could be similar to exceeding the injury threshold of mechanical loading during one's life [31]. Exceeding this threshold could occur when the mechanical load is suddenly increased or when the joint has lost its natural mechanoprotective properties.

It is generally accepted that biomechanical loading is necessary for the maintenance of cartilage homeostasis, as evidenced by the rapid loss of proteoglycans in joints that are immobilised or in disuse [32]. However, abnormal, altered or injurious loading is associated with inflammatory and metabolic imbalances that may eventually lead to OA-like damage

[13,15,33-35]. Moreover, *ex vivo* cartilage explants subjected to these magnitudes of stress exhibit a significant suppression of metabolic activity, and particularly biosynthesis of aggrecan and collagen is affected [13,15,33,34,36] similar to the *in vivo* situation [37]. Consistent upregulation of catabolic genes such as *RUNX2*, *MMP1*, *MMP3*, *MMP13* and *ADAMTS5* has been found in several mechanical injury models using either chondrocytes or cartilage explants [14,15,38-40]. The literature has shown that levels of measured genes can vary greatly, depending on the magnitude of force, speed, age of cartilage, and at which time point gene expression is measured [41-43]. In our model we measured targeted genes and in follow-up studies it would be interesting to measure the whole genomic transcript using RNA-sequencing to identify different pathways modulating the lasting response to mechanical stress. Our model applying 65% MS might be most suitable to study interventions aimed at post-traumatic OA patients who would benefit most from a reduction of the (early) response of cartilage to mechanical stress.

In our third model we showed that in response to T₃, chondrocyte signalling increased expression of the early hypertrophic markers *COL10A1* and *MMP13* (FC=5.0; $P=6.1 \times 10^{-3}$ and FC=3.7; $P=3.0 \times 10^{-3}$, respectively), while also greatly increasing the mineralization markers *COL1A1* and *ALPL* (FC=144.7; $P=3.0 \times 10^{-3}$ and FC=665.8; $P=7.4 \times 10^{-9}$, respectively). Together, these results suggest that T₃ induces terminal differentiation towards bone in chondrocytes. Treatment with T₃ also induced a greatly consistent increased gene expression of *COL2A1* (FC=3.5; $P=2.4 \times 10^{-10}$), but did not affect *ACAN* expression. Nonetheless, upregulation of *COL2A1* does not necessarily mean that T₃ induces a beneficial response of chondrocytes, as *COL2A1* is also upregulated in response to damage. In addition, a microarray study has shown that *COL2A1* gene expression is upregulated in preserved compared to healthy cartilage, suggesting that there might be an early role for *COL2A1* in the OA process when the cartilage is still trying to repair matrix damage [44]. To understand downstream transcriptional effects of T₃ we measured *RUNX2* and *EPAS1*, two critical transcription factors hallmarking OA and acting downstream of T₃. We measured an upregulation of both *EPAS1* and *RUNX2* (FC=1.8; $P=1.0 \times 10^{-3}$ and FC=1.2; $P=7.1 \times 10^{-2}$, respectively), suggesting a possible role for both transcription factors as downstream targets of T₃. The changes in chondrocyte signalling after T₃ perturbation did not lead to significant changes of cartilage matrix integrity. Our results indicate that hypertrophy was induced by T₃ in our explant model and that this was not necessarily detrimental to the cartilage matrix. T₃ can induce changes in chondrocyte signalling directly, by binding to specific thyroid responsive elements (TREs) on the DNA whereby it regulates transcription, or more indirectly by activating the transcription of another transcriptional regulator such as *RUNX2*. However, which genes are transcriptionally regulated by T₃ needs to be elucidated and regulation has been shown to be very tissue-specific because of the different levels and isotypes of thyroid hormone receptors present in different cell types. It is possible that T₃ is able to induce multiple genes such as *MMP13* in cartilage via binding to TREs. For example, in *trβ* crisprant tadpoles, T₃ did not induce *MMP13* gene expression suggesting that T₃ acts via Trβ on inducing transcription [45].

Other researchers have seen similar effects using T₃ and T₄, with T₃ being a more potent inducer of collagen production [46,47]. However, these two studies did not observe an increase in hypertrophic markers such as *COL10* and *COL1*, and this could be due to the cell type and concentration used in their experiments. On the contrary, in an *in vitro* chondrogenesis model using human bone marrow-derived stem cells (hBMSCs), perturbation with T₃ increased chondrocyte cell signalling of terminal maturation markers (*ALPL*, *COL1A1*) [37].

Overexpression of *DIO2*, encoding for the D2 enzyme which converts T4 into T3, in the same model had even more detrimental effects. This explant model perturbed by T3 might be most suitable to study interventions aimed at investigating mild types of OA that are more characterized by occurrence of hypertrophy and mineralization of cartilage.

The observation that we did not measure a response of *ADAMTS5* in our three models was unexpected. Possible explanations could be that in general expression levels of *ADAMTS5* were too low to be accurately assessed or that *ADAMTS5* expression was too heterogeneous between patients to lead to concluding results. A more biological explanation could be the temporal and tight regulation of *ADAMTS5* gene expression, peaking 10 hours after injury and declining thereafter [42].

A major strength of our models is that they consider aged, yet preserved, human osteochondral explants of a heterogeneous OA patient population. As a result cartilage explants may reflect a reliable biomimetic model, prone to OA onset. Moreover, despite the heterogeneous patient population we present consistent output specific for three different relevant triggers of OA, allowing for development of different treatment modalities. Some weaknesses of the models concern the scalability and dependency of patients undergoing joint replacement surgery. In addition, we only measured changes of the overall cartilage matrix and not changes of specific proteins that make up the articular cartilage, such as collagen type II. Nonetheless, we advocate that focusing clinical development on directly counteracting these specific unbeneficial responses of chondrocytes upon these OA triggers will facilitate further personalized development and testing of desperately needed disease modifying OA drugs. Our data provide a reference for development of advanced 3D *in vitro* model systems of cartilage, bone or osteochondral models aiming towards a joint on a chip using the sensitive changes in gene expression. Moreover, our model offers a next step opportunity for in depth molecular exploration with and without perturbations, e.g., by RNA sequencing in bulk or at the single-cell level.

Conclusions

Our study demonstrates that it is possible to set up personalized human OA disease models reflecting different relevant aspects (inflammation, hypertrophy and mechanical stress) of OA pathophysiology. The different perturbing factors and their variety in downstream effects could facilitate the development of novel targeted treatment modalities reflecting different aspects of the OA pathophysiology. Applying the here presented aged human explant model could result in a paradigm shift for biomedical research and the pharmaceutical industry leading to new ways to identify desperately needed effective drugs for OA.

Acknowledgements

Funding

The research leading to these results has received funding from the Dutch Arthritis Society/ ReumaNederland (DAF-15-4-401) and the Dutch Scientific Research council NWO /ZonMW VICI scheme (91816631/528). The Leiden University Medical Centre have and are supporting the RAAK study. The Rapid Service Fee and the Open Access fee were funded by the Dutch

Scientific Research council NWO /ZonMW VICI scheme (91816631/528).

Authors' contributions

All named authors meet the International Committee of Medical Journal Editors (ICMJE) criteria for authorship for this article, take responsibility for the integrity of the work as a whole, and have given their approval for this version to be published. Study concept and design: EH, YFM, IM. Acquisition of material and data: EH, MvH, HED, NL, EL-Z, RGHHN. Data analysis: EH, YFM and IM. Preparation of the manuscript: EH, IM. Critical reviewing and approval of the manuscript: All authors.

Disclosures

Evelyn Houtman, Marcella van Hoolwerff, Nico Lakenberg, Eka Suchiman, Enrike van der Linden – van der Zwaag, Rob Nelissen, Yolande Ramos and Ingrid Meulenbelt declare that they have no conflict of interest.

Compliance with ethics guidelines

The RAAK study has been approved by the medical ethical committee of the Leiden University Medical Center (P08.239/P19.013). Patients provided written informed consent to participate in the study and had the right to withdraw at any time.

Data availability

The datasets during and/or analysed during the current study available from the corresponding author on reasonable request.

Patients and other acknowledgments

We would like to thank all study participants of the RAAK study. We thank all the members of our group; Alejandro Rodríguez Ruiz, Ritchie Timmermans, Margo Tuerlings, Rodrigo Coutinho de Almeida and Niek Bloks. We also thank Anika Rabelink-Hoogenstraaten, Demiën Broekhuis, Robert van der Wal, Peter van Schie, Shaho Hasan, Maartje Meijer, Daisy Latijnhouwers and Geertje Spierenburg for assistance in collecting RAAK samples.

REFERENCES

1. Atkins GJ, Welldon KJ, Halbout P, et al. Strontium ranelate treatment of human primary osteoblasts promotes an osteocyte-like phenotype while eliciting an osteoprotegerin response. *Osteoporos Int.* 2009;20(4):653-64.
2. Woolf AD, Erwin J, March L. The need to address the burden of musculoskeletal conditions. *Best Pract Res Clin Rheumatol.* 2012;26(2):183-224.
3. Dreier R. Hypertrophic differentiation of chondrocytes in osteoarthritis: the developmental aspect of degenerative joint disorders. *Arthritis Res Ther.* 2010;12(5):216.
4. Pfander D, Swoboda B, Kirsch T. Expression of early and late differentiation markers (proliferating cell nuclear antigen, syndecan-3, annexin VI, and alkaline phosphatase) by human osteoarthritic chondrocytes. *Am J Pathol.* 2001;159(5):1777-83.
5. von der Mark K, Kirsch T, Nerlich A, et al. Type X collagen synthesis in human osteoarthritic cartilage. Indication of chondrocyte hypertrophy. *Arthritis Rheum.* 1992;35(7):806-11.
6. Poole AR, Nelson F, Dahlberg L, et al. Proteolysis of the collagen fibril in osteoarthritis. *Biochem Soc Symp.* 2003(70):115-23.
7. Fuerst M, Bertrand J, Lammers L, et al. Calcification of articular cartilage in human osteoarthritis. *Arthritis Rheum.* 2009;60(9):2694-703.
8. Kuhn K, D'Lima DD, Hashimoto S, et al. Cell death in cartilage. *Osteoarthritis Cartilage.* 2004;12(1):1-16.
9. Goldring MB, Goldring SR. Articular cartilage and subchondral bone in the pathogenesis of osteoarthritis. *Ann N Y Acad Sci.* 2010;1192:230-7.
10. Bird JL, Wells T, Platt D, et al. IL-1 beta induces the degradation of equine articular cartilage by a mechanism that is not mediated by nitric oxide. *Biochem Biophys Res Commun.* 1997;238(1):81-5.
11. Clutterbuck AL, Mobasheri A, Shakibaei M, et al. Interleukin-1beta-induced extracellular matrix degradation and glycosaminoglycan release is inhibited by curcumin in an explant model of cartilage inflammation. *Ann N Y Acad Sci.* 2009;1171:428-35.
12. Geurts J, Jurić D, Müller M, et al. Novel Ex Vivo Human Osteochondral Explant Model of Knee and Spine Osteoarthritis Enables Assessment of Inflammatory and Drug Treatment Responses. *International Journal of Molecular Sciences.* 2018;19(5):1314.
13. Kurz B, Jin M, Patwari P, et al. Biosynthetic response and mechanical properties of articular cartilage after injurious compression. *J Orthop Res.* 2001;19(6):1140-6.
14. Chan PS, Schlueter AE, Coussens PM, et al. Gene expression profile of mechanically impacted bovine articular cartilage explants. *J Orthop Res.* 2005;23(5):1146-51.
15. Quinn TM, Grodzinsky AJ, Hunziker EB, et al. Effects of injurious compression on matrix turnover around individual cells in calf articular cartilage explants. *J Orthop Res.* 1998;16(4):490-9.
16. Bomer N, den Hollander W, Ramos YF, et al. Translating genomics into mechanisms of disease: Osteoarthritis. *Best Pract Res Clin Rheumatol.* 2015;29(6):683-91.
17. Lv M, Zhou Y, Polson SW, et al. Identification of Chondrocyte Genes and Signaling Pathways in Response to Acute Joint Inflammation. *Sci Rep.* 2019;9(1):93.
18. Vincent TL. IL-1 in osteoarthritis: time for a critical review of the literature. *F1000Res.* 2019;8.
19. Mackay AM, Beck SC, Murphy JM, et al. Chondrogenic differentiation of cultured human mesenchymal stem cells from marrow. *Tissue Eng.* 1998;4(4):415-28.
20. Mueller MB, Tuan RS. Functional characterization of hypertrophy in chondrogenesis of human mesenchymal stem cells. *Arthritis Rheum.* 2008;58(5):1377-88.
21. Sanchez-Adams J, Leddy HA, McNulty AL, et al. The mechanobiology of articular cartilage: bearing the burden of osteoarthritis. *Curr Rheumatol Rep.* 2014;16(10):451.
22. Farndale RW, Buttle DJ, Barrett AJ. Improved quantitation and discrimination of sulphated glycosaminoglycans by use of dimethylmethylene blue. *Biochim Biophys Acta.* 1986;883(2):173-7.
23. Mankin HJ, Dorfman H, Lippiello L, et al. Biochemical and metabolic abnormalities in articular cartilage from osteo-arthritic human hips. II. Correlation of morphology with biochemical and metabolic data. *J Bone Joint Surg Am.* 1971;53(3):523-37.
24. Soulhat J, Buschmann MD, Shirazi-Adl A. A fibril-network-reinforced biphasic model of cartilage in unconfined compression. *J Biomech Eng.* 1999;121(3):340-7.

25. McCulloch RS, Ashwell MS, O'Nan AT, et al. Identification of stable normalization genes for quantitative real-time PCR in porcine articular cartilage. *J Anim Sci Biotechnol*. 2012;3(1):36.
26. Al-Sabah A, Stadnik P, Gilbert SJ, et al. Importance of reference gene selection for articular cartilage mechanobiology studies. *Osteoarthritis Cartilage*. 2016;24(4):719-30.
27. Saito T, Fukai A, Mabuchi A, et al. Transcriptional regulation of endochondral ossification by HIF-2 α during skeletal growth and osteoarthritis development. *Nat Med*. 2010;16(6):678-86.
28. Yang S, Kim J, Ryu JH, et al. Hypoxia-inducible factor-2 α is a catabolic regulator of osteoarthritic cartilage destruction. *Nat Med*. 2010;16(6):687-93.
29. Bohensky J, Terkhorst SP, Freeman TA, et al. Regulation of autophagy in human and murine cartilage: hypoxia-inducible factor 2 suppresses chondrocyte autophagy. *Arthritis Rheum*. 2009;60(5):1406-15.
30. Pelletier JP, Mineau F, Ranger P, et al. The increased synthesis of inducible nitric oxide inhibits IL-1 α synthesis by human articular chondrocytes: possible role in osteoarthritic cartilage degradation. *Osteoarthritis and cartilage*. 1996;4(1):77-84.
31. Vincent TL, Wann AKT. Mechanoadaptation: articular cartilage through thick and thin. *J Physiol*. 2019;597(5):1271-81.
32. Sun HB. Mechanical loading, cartilage degradation, and arthritis. *Ann NY Acad Sci*. 2010;1211:37-50.
33. Patwari P, Cook MN, DiMicco MA, et al. Proteoglycan degradation after injurious compression of bovine and human articular cartilage in vitro: interaction with exogenous cytokines. *Arthritis Rheum*. 2003;48(5):1292-301.
34. Patwari P, Cheng DM, Cole AA, et al. Analysis of the relationship between peak stress and proteoglycan loss following injurious compression of human post-mortem knee and ankle cartilage. *Biomech Model Mechanobiol*. 2007;6(1-2):83-9.
35. Guilak F. Biomechanical factors in osteoarthritis. *Best Pract Res Clin Rh*. 2011;25(6):815-23.
36. Guilak F, Meyer BC, Ratcliffe A, et al. The effects of matrix compression on proteoglycan metabolism in articular cartilage explants. *Osteoarthritis and cartilage*. 1994;2(2):91-101.
37. Bomer N, den Hollander W, Ramos YF, et al. Underlying molecular mechanisms of DIO2 susceptibility in symptomatic osteoarthritis. *Annals of the rheumatic diseases*. 2015;74(8):1571-9.
38. Riegger J, Joos H, Palm HG, et al. Antioxidative therapy in an ex vivo human cartilage trauma-model: attenuation of trauma-induced cell loss and ECM-destructive enzymes by N-acetyl cysteine. *Osteoarthritis and cartilage*. 2016;24(12):2171-80.
39. Tetsunaga T, Nishida K, Furumatsu T, et al. Regulation of mechanical stress-induced MMP-13 and ADAMTS-5 expression by RUNX-2 transcriptional factor in SW1353 chondrocyte-like cells. *Osteoarthritis and cartilage*. 2011;19(2):222-32.
40. Ashwell MS, Gonda MG, Gray K, et al. Changes in chondrocyte gene expression following in vitro impaction of porcine articular cartilage in an impact injury model. *J Orthop Res*. 2013;31(3):385-91.
41. Madej W, van Caam A, Blaney Davidson EN, et al. Physiological and excessive mechanical compression of articular cartilage activates Smad2/3P signaling. *Osteoarthritis and cartilage*. 2014;22(7):1018-25.
42. Lee JH, Fitzgerald JB, Dimicco MA, et al. Mechanical injury of cartilage explants causes specific time-dependent changes in chondrocyte gene expression. *Arthritis Rheum*. 2005;52(8):2386-95.
43. Fitzgerald JB, Jin M, Dean D, et al. Mechanical compression of cartilage explants induces multiple time-dependent gene expression patterns and involves intracellular calcium and cyclic AMP. *J Biol Chem*. 2004;279(19):19502-11.
44. Ramos YF, den Hollander W, Bovee JV, et al. Genes involved in the osteoarthritis process identified through genome wide expression analysis in articular cartilage; the RAAK study. *PLoS One*. 2014;9(7):e103056.
45. Sakane Y, Iida M, Hasebe T, et al. Functional analysis of thyroid hormone receptor beta in *Xenopus tropicalis* founders using CRISPR-Cas. *Biol Open*. 2018;7(1).
46. Whitney GA, Kean TJ, Fernandes RJ, et al. Thyroxine Increases Collagen Type II Expression and Accumulation in Scaffold-Free Tissue-Engineered Articular Cartilage. *Tissue Eng Part A*. 2018;24(5-6):369-81.
47. Glade MJ, Kanwar YS, Stern PH. Insulin and thyroid hormones stimulate matrix metabolism in primary cultures of articular chondrocytes from young rabbits independently and in combination. *Connect Tissue Res*. 1994;31(1):37-44.

Supplementary Files

List of contents:

Supplementary Tables

Table S1. Baseline information of the donors included in the three perturbations.

Table S2. Primer sequence used to determine gene expression levels in real-time PCR.

Table S3. Gene expression after treatment with IL-1 β in combination with 30% loading

Table S4. Gene expression after treatment with T3 in combination with 30% mechanical loading.

Supplementary Figures

Figure S1. Gene expression after treatment with IL-1 β in combination with 30% mechanical loading.

Figure S2. Gene expression after treatment with T3 in combination with 30% mechanical loading.

Figure S3. sGAG concentration in the media of osteochondral explants on day 3 and 6.

Figure S4. Sub categories of the Mankin Score of cartilage after treatment with either IL-1 β , T3 or 65% mechanical stress.

Figure S5. Macroscopical pictures of osteochondral explants after 65% mechanical stress (65% MS) is applied and controls.

Supplementary Tables

Table S1 | Baseline information of the donors included in the three perturbations. Characteristics of donors included in the three different perturbation models. The table represents the age, sex, and BMI per treatment group on the day of joint replacement surgery. Age and BMI are represented as average with standard deviations.

	IL-1β	T3	65% mechanical stress (MS)
N (donors)	3	8	9
F/M	3/0	4/4	3/6
(% F)	100%	50%	33%
Mean age	62.3 \pm 9.0	66.6 \pm 9.5	65.1 \pm 8.8
(range)	55-75	53-81	53-81
Mean BMI	28.9 \pm 7.9	25.9 \pm 2.4	27.9 \pm 3.4
(range)	22.5-40.1	22.5-31.2	24.8-35.1

Legend: F=Females, M=Males; age given in years

Table S2 | Primer sequence used to determine gene expression levels in real-time PCR.

Gene	Forward (F) and reverse (R) primers (5' to 3')
<i>SDHA</i>	F: TGGAGCTGCAGAACCTGATG
	R: TGTAGTCTTCCCTGGCATGC
<i>MMP13</i>	F: TTGAGCTGGACTCATTGTGCG
	R: GGAGCCTCTCAGTCATGGAG
<i>ADAMTS5</i>	F: TGGCTCACGAAATCGGACAT
	R: GCGCTTATCTTCTGTGGAACC
<i>EPAS1</i>	F: ACAGGTGGAGCTAACAGGAC
	R: CCGTGCACCTCATCCTCATG
<i>COL2A1</i>	F: CTACCCCAATCCAGCAAACGT
	R: AGGTGATGTTCTGGGAGCCTT
<i>ACAN</i>	F: AGAGACTCACACAGTCGAAACAGC
	R: CTATGTTACAGTGCTCGCCAGTG
<i>COL1A1</i>	F: GTGCTAAAGGTGCCAATGGT
	R: ACCAGGTTACCCGCTGTTAC
<i>COL10A1</i>	F: GGCAACAGCATTATGACCCA
	R: TGAGATCGATGATGGCACTCC
<i>ALPL</i>	F: CAAAGGCTTCTTCTGCTGGTG
	R: CCTGCTGGCTTTTCCITCA
<i>RUNX2</i>	F: CTGTGGTTACTGTCATGGCG
	R: AGGTAGTACTTGGGGAGGA

Table S3 | Gene expression after treatment with IL-1 β in combination with 30% loading.

Gene	Control vs IL1 β			Control vs 30% MS			Control vs IL1 β + 30% MS			Merged groups		
	Beta	SE	P-value	Beta	SE	P-value	Beta	SE	P-value	Beta	SE	P-value
MMP13	4.2	1.7	1.3x10 ⁻²	0.2	3.4	NS	0.4	1.8	NS	3.7	1.8	3.6x10 ⁻²
ADAMTSS	0.6	0.8	NS	0.3	0.7	NS	0	0.8	NS	0.2	0.5	NS
EPAS1	1.9	1.4	NS	-0.6	1.6	NS	1.8	1.5	NS	2.2	1	3.6x10 ⁻²
ACAN	-5.8	0.7	2.6x10 ⁻¹⁷	-0.7	0.7	NS	-5.3	0.8	3.6x10 ⁻¹²	-5.2	0.6	1.1x10 ⁻¹⁹
COL2A1	-7.3	0.7	2.9x10 ⁻¹³	-0.7	0.4	NS	-7.4	0.3	1.4x10 ⁻¹³	-7	0.5	2.6x10 ⁻¹²
COL10A1	-0.4	1.5	NS	0.9	1.8	NS	-0.9	1.4	NS	-1	1.3	NS
COL1A1	-2	3.3	NS	-2.7	3.9	4.8x10 ⁻²	-3.4	3.6	NS	-1.4	2.6	NS
ALP	0.8	3	NS	-1.8	3.7	NS	-2.8	2.8	NS	-0.1	2.2	NS

Table S3: Gene expression after treatment with IL-1 β in combination with 30% loading. RT-PCR analysis of MMP13, ADAMTS, COL2A1, ACAN, COL1A1, COL10A1, ALPL gene expression comparing [first column] IL-1 β (n=3) versus controls (n=3), [second column] 30% MS (n=3) to controls (n=3), [third column] IL-1 β +30% MS (n=3) versus controls (n=3) and [fourth column] Control and 30% MS merged (n=6) versus IL-1 β and IL-1 β +30% MS merged (n=6). Beta is determined by the GEE during the modelling and represents the difference between the perturbation and control groups.

Table S4 | Gene expression after treatment with T3 in combination with 30% mechanical loading.

Gene	Control vs T3			Control vs 30% MS			Control vs T3 + 30% MS			Merged groups		
	Beta	SE	P-value	Beta	SE	P-value	Beta	SE	P-value	Beta	SE	P-value
MMP13	1.3	0.6	3.9x10 ⁻²	-0.2	1.2	NS	2	0.7	5.0x10 ⁻³	1.7	0.6	3.0x10 ⁻³
ADAMTS5	0.2	1	NS	1	0.8	NS	0.9	1	NS	0.2	0.8	NS
EPAS1	1	0.3	1.0x10 ⁻³	0.9	0.3	4.0x10 ⁻³	1.3	0.4	4.1x10 ⁻⁴	0.8	0.3	1.0x10 ⁻³
ACAN	0.5	0.6	NS	0.9	0.5	4.3x10 ⁻²	1.5	0.5	2.0x10 ⁻³	0.6	0.4	NS
COL2A1	1.9	0.5	3.5x10 ⁻⁵	-0.2	0.4	NS	2.2	0.4	2.2x10 ⁻⁷	2.1	0.3	2.4x10 ⁻¹⁰
COL10A1	1.6	0.6	5.0x10 ⁻³	-0.1	0.7	NS	1	0.6	NS	1.3	0.5	3.0x10 ⁻³
COL1A1	1.9	0.9	4.2x10 ⁻²	-2.1	1.6	NS	1.6	1.2	NS	2.4	0.9	6.1x10 ⁻³
ALP	4.2	0.9	3.0x10 ⁻⁶	-1.9	1.9	NS	4.5	1	3.0x10 ⁻⁶	4.9	0.8	7.4x10 ⁻⁹

Table S4. Gene expression after treatment with T3 in combination with 30% mechanical loading. RT-PCR analysis of MMP13, ADAMTS, COL1A1, ACAN, COL10A1, COL1A1, ALPL gene expression comparing [first column] T3 (n=12) versus controls (n=15), [second column] 30% MS (n=6) to controls (n=15), [third column] T3+30% MS (n=9) versus controls (n=15) and [fourth column] Control and 30% MS merged (n=21) versus T3 and T3+30% MS merged (n=21). Beta is determined by the GEE during the modelling and represents the

Supplementary Figures

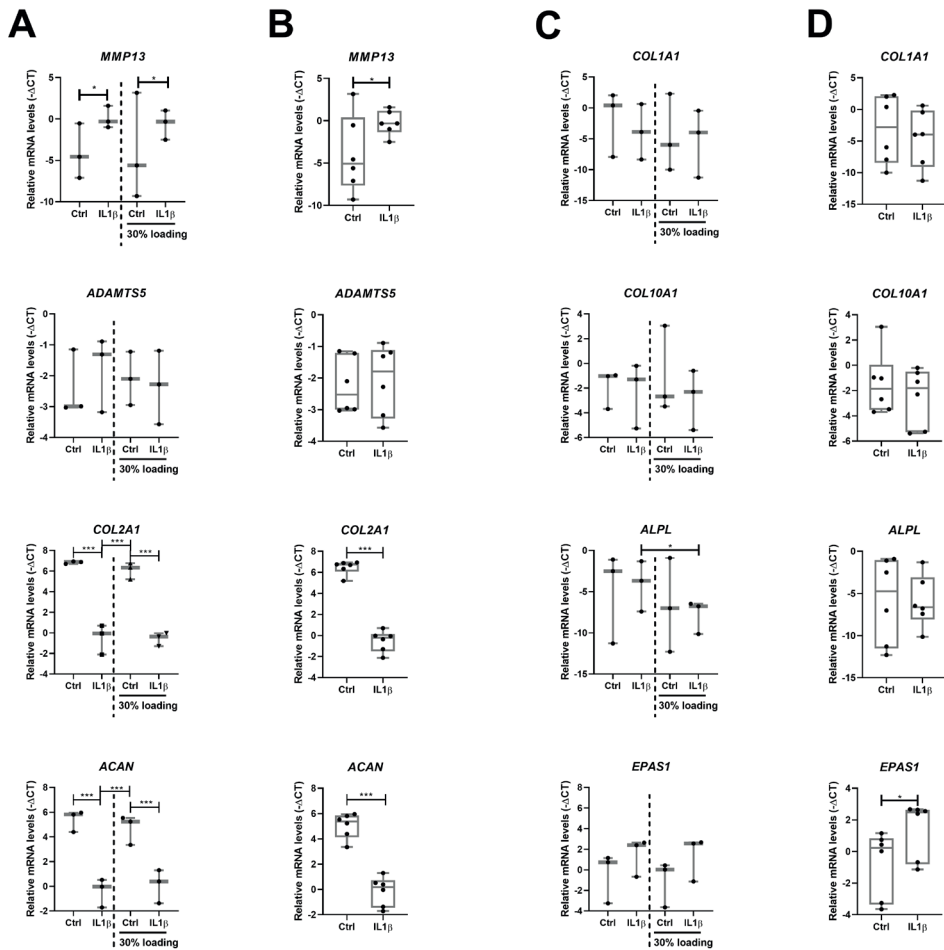


Figure S1 | Gene expression after treatment with IL-1 β in combination with 30% mechanical loading. RT-PCR analysis of MMP13, ADAMTS, COL2A1 and ACAN after **[A]** IL-1 β (10 ng/ml; n=3), 30% loading (n=3) and IL-1 β +30% loading (10 ng/ml; n=3), **[B]** Control and 30% loading merged (n=6) versus IL-1 β and IL-1 β +30% loading merged (10 ng/ml; n=6). RT-PCR analysis of COL1A1, COL10A1, ALPL and EPAS1 after **[C]** IL-1 β (10 ng/ml; n=3), 30% loading (n=3) and IL-1 β +30% loading (10 ng/ml; n=3) **[D]** Control and 30% loading merged (n=6) versus IL-1 β and IL-1 β +30% loading merged (10 ng/ml; n=6). Data is presented in a boxplot depicting the median, lower and upper quartiles and each black dot represents a single explant. *P<0.05, **P<0.01, ***P<0.001.

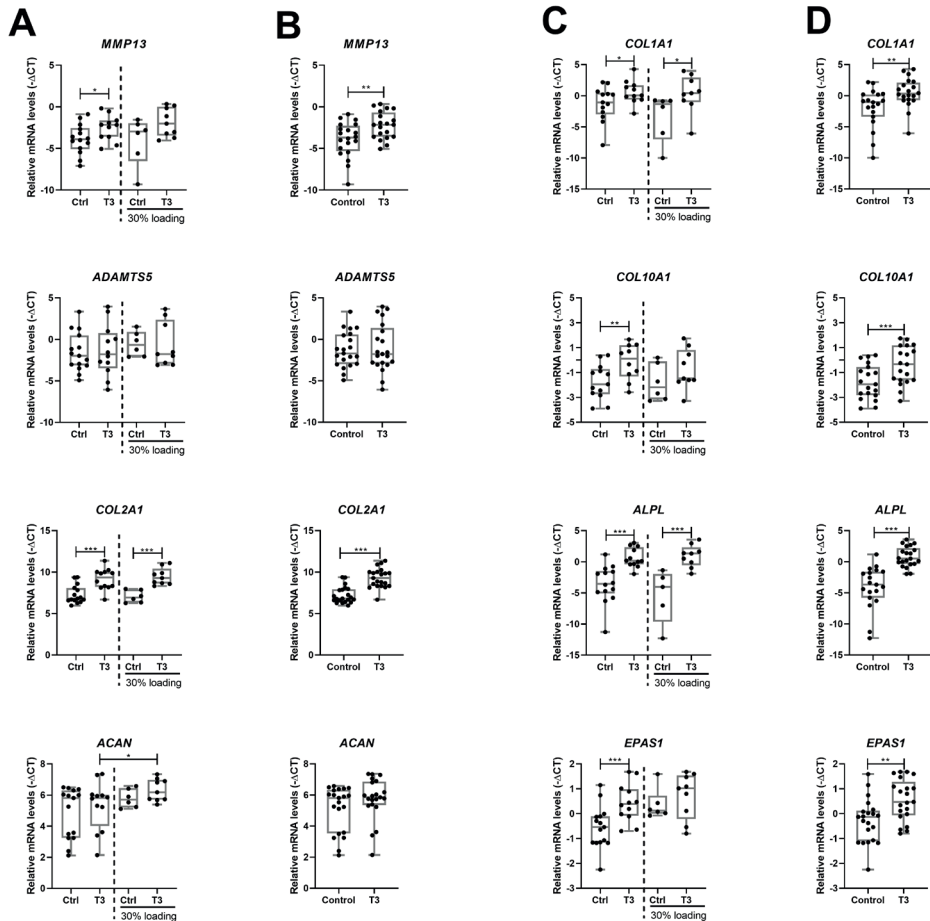


Figure S2 | Gene expression after treatment with T3 in combination with 30% mechanical loading. RT-PCR analysis of MMP13, ADAMTS, COL2A1 and ACAN after **[A]** T3 (10 nM; n=12), 30% loading (n=6) and T3+30% loading (10 nM; n=9), **[B]** Control and 30% loading merged (n=21) versus T3 and T3+30% loading merged (10 nM; n=21). RT-PCR analysis of COL1A1, COL10A1, ALPL and EPAS1 after **[C]** T3 (10 nM; n=12), 30% loading (n=6) and T3+30% loading (10 nM; n=9) **[D]** Control and 30% loading merged (n=21) versus T3 and T3+30% loading merged (10 nM; n=21). Data is presented in a boxplot depicting the median, lower and upper quartiles and each black dot represents a single explant. * $P < 0.05$, ** $P < 0.01$, *** $P < 0.001$.

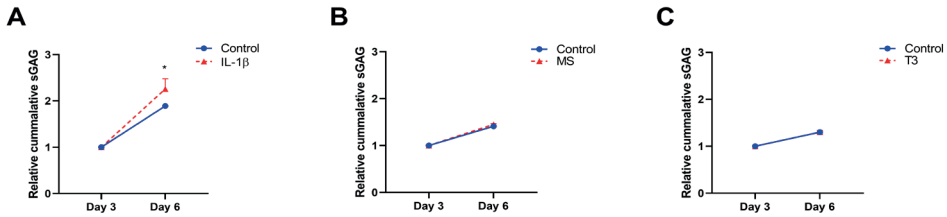


Figure S3 | sGAG concentration in the media of osteochondral explants on day 3 and 6. Cumulative sGAG released relative to day 3 levels from cartilage into conditioned media of osteochondral explants in presence of **[A]** IL-1 β (10ng/ml; n=2), **[B]** MS (n=13-17) or **[C]** T3 (10nM; n=7-9) as determine by the DMMB assay. Data is represented as mean \pm s.e.m. *P<0.05, **P<0.01. S.e.m.<0.05 are not distinguishable in the figure.

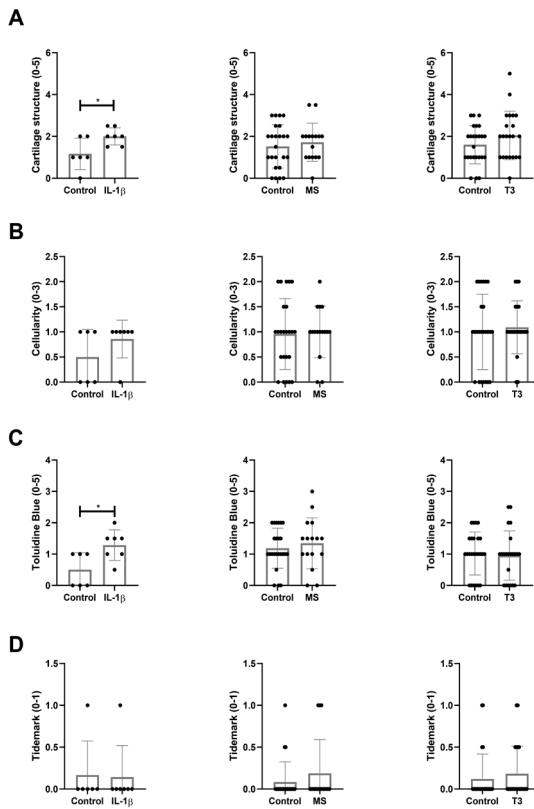


Figure S4 | Sub categories of the Mankin Score of cartilage after treatment with either IL-1 β , T3 or 65% mechanical stress. Cartilage damage was assessed after perturbation with IL-1 β (n=6), 65% MS (n=16/24) or T3 (n=22/24) with a modified Mankin Score. In this scoring system cartilage was scored based on **[A]** cartilage structure, **[B]** cellularity, **[C]** loss of sGAG in toluidine blue stainings and **[D]** tidemark integrity. Data is represented as mean \pm s.e.m and each black dot represents a single explant. *P<0.05, **P<0.01, ***P<0.001.

2

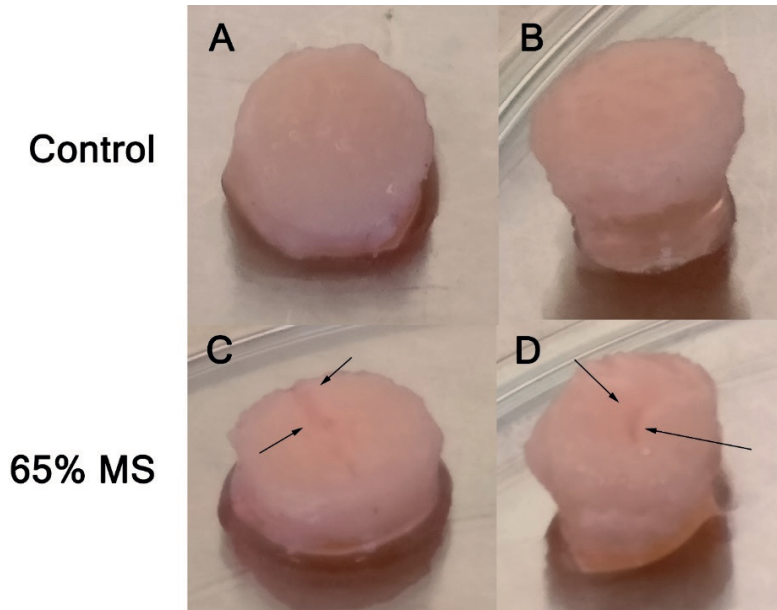


Figure S5. Macroscopical pictures of osteochondral explants after 65% mechanical stress (65% MS) is applied and controls. Prior to harvest on day 13, pictures were taken of the cartilage surface of all osteochondral explants. **[A and B]** Photograph of control osteochondral explants show no major abnormalities on the cartilage surface. **[C and D]** Photograph of 65% mechanical stressed osteochondral explants. Arrows indicate visible cartilage fissures and cracks.

